Monthly Notices
of the
ROYAL ASTRONOMICAL SOCIETY

MNRAS **484,** 204–217 (2019)
Advance Access publication 2019 January 2

doi:10.1093/mnras/sty3526

The space density of $z > 4$ blazars

A. Caccianiga,[1★] A. Moretti,[1] S. Belladitta,[1,2] R. Della Ceca,[1] S. Antón,[3] L. Ballo,[4] C. Cicone,[1] D. Dallacasa,[5,6] A. Gargiulo,[7] L. Ighina,[1,8] M. J. Marchã[9] and P. Severgnini[1]

[1]*INAF - Osservatorio Astronomico di Brera, via Brera 28, I-20121 Milan, Italy*
[2]*DiSAT, Università degli Studi dell'Insubria, Via Valleggio 11, I-22100 Como, Italy*
[3]*CIDMA, Department of Physics, University of Aveiro, 3810-193, Aveiro, Portugal*
[4]*XMM-Newton Science Operations Centre, ESAC/ESA, PO Box 78, E-28691 Villanueva de la Caãda, Madrid, Spain*
[5]*Dipartimento di Astronomia, Università di Bologna, via Ranzani 1, I-40127, Bologna, Italy*
[6]*INAF - Istituto di Radioastronomia, Via Gobetti 101, I-40129 Bologna, Italy*
[7]*INAF - Istituto di Astrofisica Spaziale e Fisica Cosmica (IASF), Via E. Bassini 15, I-20133 Milano, Italy*
[8]*Dipartimento di Fisica G. Occhialini, Università di Milano-Bicocca, Piazza della Scienza 3, I-20126 Milano, Italy*
[9]*Department of Physics & Astronomy, University College London, Gower Street, London, WC1E 6BT, UK*

Accepted 2018 December 20. Received 2018 December 20; in original form 2018 November 13

ABSTRACT

High-redshift blazars are an important class of active galactic nuclei (AGN) that can provide an independent estimate of the supermassive black hole mass function in high-redshift radio-loud AGN without the bias due to absorption along the line of sight. Using the Cosmic Lens All Sky Survey (CLASS), we built a complete radio flux-limited sample of high-redshift ($z > 4$) blazars suitable for statistical studies. By combining dedicated optical observations and the SDSS spectroscopic database, we obtained a sample of 26 blazar candidates with a spectroscopic redshift above 4. On the basis of their radio spectrum, we distinguish between blazars and QSO with a Gigahertz Peaked Spectrum (GPS) like spectrum. Out of the 18 confirmed blazars 14 constitute a completely identified, flux-limited sample down to a magnitude of 21 (AB). Using this complete sample, we derive a space density of blazars with $4 < z < 5.5$ of $\rho = 0.13^{+0.05}_{-0.03}$ Gpc^{-3}. This is the first actual estimate of the blazar space density in this range of redshift. This value is in good agreement with the extrapolation of the luminosity function and cosmological evolution based on a sample of flat-spectrum radio quasars selected at lower redshifts and it is consistent with a cosmological evolution peaking at $z \sim 2$ similar to radio-quiet QSO. We do not confirm, instead, the presence of a peak at $z \sim 4$ in the space density evolution, recently suggested using an X-ray selected sample of blazars. It is possible that this extreme peak of the evolution is present only among the most luminous blazars.

Key words: galaxies: active – galaxies: high-redshift – galaxies: nuclei.

1 INTRODUCTION

Supermassive black holes (SMBH) are the result of the evolution of the mass inflow towards the nuclear region of galaxies across cosmic time (see Merloni 2016 for a recent review). A fundamental question is how the observed local population of SMBH can be traced back to the original seeds through different phases of growth, identified by the intense nuclear accretion activity (AGN). High-redshift AGN surveys represent the best tool to provide observational constraints to current theoretical models of SMBH formation (e.g. Volonteri 2010; Valiante et al. 2017). New surveys planned for the next decades will play a fundamental role in this field by selecting thousands of high-z AGN. However, obscuration from circumnuclear matter is expected to introduce selection biases that are difficult to quantify (see e.g. McGreer et al. 2006; Zeimann et al. 2011; Vito et al. 2018). Radio selections, like those that will be carried out with Square Kilometre Array (SKA) or with its precursors (see e.g. Norris et al. 2011), can provide a less biased census of high-z AGN (at least of the radio-loud fraction) since radio wavelengths are unaffected by absorption. This is true, however, only if the selection of the high-z radio sources is not based on the colours of the optical counterparts otherwise the usual biases against absorbed AGN will be present also in these samples.

★ E-mail: alessandro.caccianiga@brera.inaf.it

A complementary approach has been recently proposed (Volonteri et al. 2011; Ghisellini et al. 2014; Sbarrato et al. 2015) based on the class of blazars, i.e. radio-loud AGN whose relativistic jet points towards the observer (Urry & Padovani 1995). The particular orientation of these sources makes obscuration less important, since the jet is expected to clear out the path along the line of sight to the active nucleus and the dusty torus should not intercept the radiation. Another advantage of studying blazars is that their compact radio emission is less affected by the attenuation due to the interaction of radio photons with the cosmic microwave background (CMB) if compared to the mis-aligned, lobe-dominated radio-loud AGN (see e.g. Ghisellini et al. 2015, Wu et al. 2017). The space density of the entire population of radio-loud AGN can then be inferred indirectly from the observed number of blazars since we expect: $N_{\rm total} = N_{\rm blazars} \times 2\Gamma^2$, where Γ is the Lorentz factor of the bulk velocity in the jet (typically, $\Gamma \sim$10–15; e.g. Ghisellini et al. 2014).

The use of blazars to study the high-redshift Universe requires the selection of well-defined and sizable samples suitable for reliable statistical analyses. Sbarrato et al. (2013) used a systematic approach to select a well-defined sample of high-z blazars starting from the $z > 4$ QSO present in the SDSS (DR7) and considering only the most radio-loud ones that are expected to be mostly blazars. The recognition of the actual blazars in the sample is in progress. With this approach, Sbarrato et al. (2013) are building up an *optically selected* sample of blazars whose completeness is related to the actual completeness of the starting data set (the SDSS DR7 spectroscopic database).

Here, we present an alternative (and complementary) approach aimed at building a *radio-flux limited* sample of high-z (z>4) blazars to be directly comparable with radio samples selected at lower redshifts. We do not limit our search to the SDSS sky area and to the already available spectroscopic identifications. The starting point is the Cosmic Lens All Sky Survey (CLASS; Myers et al. 2003; Browne et al. 2003), a flux density limited survey at 5 GHz ($S_{\rm 5GHz} > 30$ mJy) covering almost the entire Northern hemisphere (16 300 deg^2) and that contains 11 000 flat spectrum radio sources. The goal is to create the largest radio-selected sample of bona fide high-z blazars to be used for statistically sound studies. Since blazars have flat radio spectra, this survey represents the ideal starting point for an efficient selection. CLASS is also deep enough to allow the detection of powerful (10^{27} W Hz^{-1}) blazars at z = 5–6. Using existing spectra (mostly from SDSS) *plus* dedicated observing runs at 4–10 meter class telescopes we have now completed (at 95 per cent level) the identification of the sample down to a well-defined optical magnitude (21) in a filter corresponding to a rest frame 1200–1400Å wavelength range (i.e. either r, i, or z filter depending on the redshift of the source).

In this paper, we present this sample together with a first estimate of the space density of blazars in the 4–5.5 redshift bin. In Section 2, we discuss how the sample has been selected while in Section 3 we present the spectroscopic follow-up that we have recently carried out to complete the identification of the high-z candidates. The completeness of the sample is studied in Section 4. We then use (Section 5) the radio spectral indices over a wide range of frequencies, from 150 MHz up to 8.4 GHz, to distinguish between genuine flat-spectrum radio sources from steep spectrum objects or sources with a peaked spectrum. We finally derive the volume density of blazars versus redshift (between 4 and 5.5, Section 6) and compare it with the predictions based on samples selected at lower redshifts (Section 7). Conclusions are reported in Section 8.

Throughout the paper, we assume a flat ΛCDM cosmology with $H_0 = 70\,{\rm km\,s^{-1}\,Mpc^{-1}}$, $\Omega_\Lambda = 0.7$, and $\Omega_{\rm M} = 0.3$. Spectral indices are given assuming $S_\nu \propto \nu^{-\alpha}$.

2 THE CLASS SAMPLE OF HIGH-z AGN CANDIDATES

CLASS is a flux limit survey at 5 GHz of flat spectrum radio sources, covering most of the northern sky (16 300 deg^2). It was built by combining the NRAO VLA Sky Survey (NVSS), at 1.4 GHz (Condon et al. 1998), with the Green-Bank Survey, GB6, at 5 GHz (Gregory et al. 1996) and by selecting only the objects with a flat spectrum between 1.4 and 5 GHz (α <0.5, with $f_\nu \propto \nu^{-\alpha}$). All the selected sources have been then followed-up at 8.4 GHz using the Very Large Array (VLA) in its most extended configuration (A-array) providing a resolution of 0.2 arcsec. The VLA follow-up provided not only a flux density at relatively high frequency but also a very accurate (sub-arcsec) radio position. CLASS represents the ideal starting point for an efficient selection since blazars have flat radio spectra. In addition, the availability of radio positions with uncertainties below a fraction of arcsecond guarantees the detection of the correct counterpart, even at faint optical magnitudes, without significant spurious contamination. In particular, we use a search radius of 0.6 arcsec to find the optical counterpart of the CLASS sources.

First searches for high-z AGN from the CLASS survey started more than 15 yr ago using the relatively shallow optical data available at that time (e.g. Snellen et al. 2001). Thanks to the recent release of the Panoramic Survey Telescope and Rapid Response System (Pan-STARRS1, PS1) survey (Chambers et al. 2016), we have now an almost complete coverage of relatively deep photometric data in five bands (g, r, i, z, and Y). Besides PS1 data we have also a complete coverage at mid-Infrared wavelengths from the Wide-field Infrared Survey Explorer (WISE; Wright et al. 2010). We use all these photometric data to select high-z ($z > 4$) AGN candidates in CLASS through the detection of the drop in the continuum flux when the Ly α forest and the Lyman limit systems enter a photometric filter (dropout method) . This effect produces a very red colour between two filters, typically $g-r$, $r-i$, or $i-z$ (for the range of redshift between 4 and 6, considered here). In order to obtain the highest level of completeness, we require that the $g-r$, $r-i$, or $i-z$ are larger than 1.1 (see Fig. 1 and Fig. 2). This threshold is suggested by the expected colours of a typical QSO template (see Fig. 2) and it has been set so as to include the large majority (>99 per cent) of the $z > 4$ QSO discovered to date, as shown in Fig. 2.

A common contaminant for this type of selection are the dwarf stars. Usually, to minimize the inclusion of these contaminants it is often imposed an additional constraint on the colours of the source. For instance, for a g-dropout object it is usually required a blue colour between r and i filters, while for an r-dropout source it is required a blue i–z (see e.g. Fan et al. 2000, 2003). However, this can introduce some incompleteness in the selection. Therefore, we decided not to apply such a constraint also supported by the fact that a radio selection excludes, by definition, the contamination from stars. The most important type of contamination in the case of a radio-selected sample are low-redshift ($z \sim$ 1–2) 'red' (i.e. moderately absorbed) AGN. This contamination can be kept at minimum using mid-IR data from WISE since low-redshift red AGN typically have stronger 3 micron (observer's frame) emission (W2 magnitude) than high-redshift objects with the same magnitude in the z filter. In particular, we impose that the object is either undetected in WISE

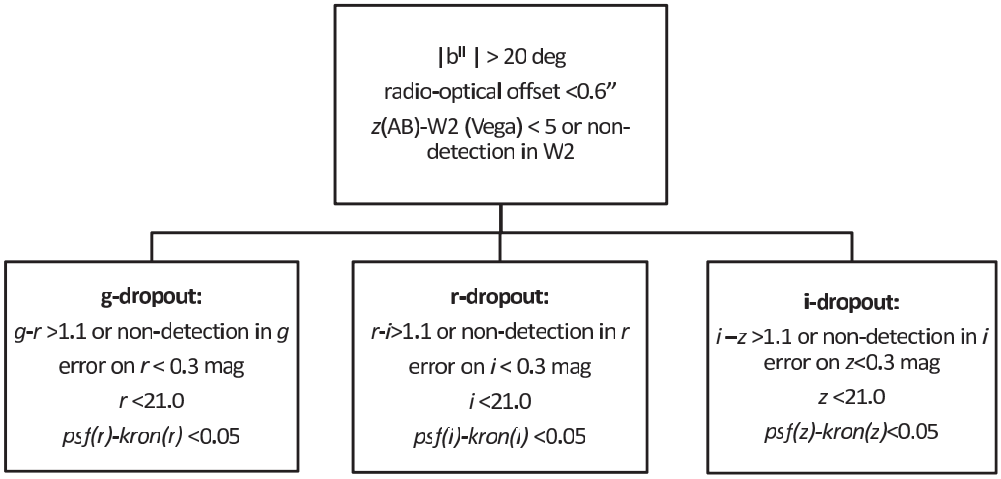

Figure 1. Summary of the criteria adopted to select high-z candidates from the CLASS survey (see the text for details).

(W2) or, if detected, we require that $z-\mathrm{W2} < 5$.[1] This threshold, which is very similar to the one adopted by Carnall et al. (2015) to search for high-redshift QSO ($z-\mathrm{W2} < 4.5$), includes virtually all the known high-z QSO (see Fig. 2)

Finally, we require that the source is star-like (psf magnitude−kron magnitude<0.05; see Chambers et al. 2016) and that the magnitude in the reddest filter of each selection (i.e. r magnitude for $g-r$ selection, the i magnitude for the $r-i$ selection and the z magnitude for the $i-z$ selection) is brighter than 21. This last constraint guarantees that the dropout is significant when the object is not detected in the bluest filter. The fact that the magnitude limit (AB system) is the same in the three selections simplifies the statistical analysis of the sample since it corresponds to a uniform threshold in the rest-frame wavelength interval of 1200–1400 Å for all the selected objects.

To reduce the number of possible spurious optical counterparts, we further restricted the search area to the high Galactic latitudes ($|\ b^{II}\ | \geq 20$ deg). The adopted selection criteria are summarized in Fig. 1.

After this selection, we inspected the high-z candidates and removed all the problematic cases (i.e. sources close to bright stars and/or with photometric problems). The complete list of high-z candidates selected in CLASS is presented in Table 1. This list includes 37 objects out of which 25 have either a spectroscopic redshift from the literature or an available optical spectrum in the Sloan Digital Sky Survey (SDSS) catalogue. Nearly all the objects with an identification or an optical spectrum from SDSS are high-z QSO with z above 3 except for 1 BL Lac object (GB6J154929 + 170853) that is probably at $z \sim 1.2$, based on a tentative detection of MgIIλ2798Å ($z \sim 1.25$) and CIII]λ1909Å ($z \sim 1.16$).[2] In any case, the optical spectrum of GB6J154929 + 170853 is clearly 'blue' with no obvious signs of dropout. In the SDSS (DR13) catalogue, the $g-r$ is much lower (0.4 mag) than what is reported in the PS1 catalogue (>4). This is likely a case of problematic photometry in the PS1.

[1]We use the PSF magnitudes provided by PS1, that are in AB system, and the magnitudes from allwise catalogue, that are in Vega system

[2]SDSS reports $z = 0.62$, in DR13 and DR14, and $z = 3.39$ in DR12. None of these tentative redshifts have convincing correspondences with the possible features observed in the spectrum and, therefore, we consider them unreliable.

The remaining 12 selected candidates needed a spectroscopic follow-up. To this end, we carried out dedicated observations at Large Binocular Telescope (LBT) and at the Telescopio Nazionale Galileo (TNG) as detailed in the following section.

3 THE SPECTROSCOPIC OBSERVATIONS

During 2017–2018, we have carried out dedicated spectroscopic observations of the high-z blazar candidates of CLASS using the LBT and the TNG. In the following, we give some detail on these observing runs. The new spectroscopic identifications collected at these telescopes are reported in Table 1.

LBT. LBT has a binocular design with two identical 8.4 meter telescopes and it is located on Mount Graham, Arizona (US). For our project, we used LBT coupled to the Multi-Object Double Spectrograph (MODS; Pogge et al. 2010). The observations were taken during the period 2017 November–2018 May with the red grating (G670L, 5 000–10 000Å) and using slit widths of 1–1.2 arcsec. Data reduction was performed at the Italian LBT Spectroscopic Reduction Center through scripts optimized for LBT data. Each spectral image was independently bias subtracted and flat-field corrected. Sky subtraction was done on 2D extracted, wavelength calibrated spectra with a fit. Wavelength calibration was obtained from spectra of arc lamps (rms = 0.08 Å on MODS1 and 0.1 Å on MODS2), while flux calibration was achieved from observations of a spectro-photometric standard.

TNG. The TNG telescope is a 3.58-m telescope located in the island of San Miguel de La Palma (Spain). We carried out the observations in March and in 2018 May using DOLORES (Device Optimized for the LOw RESolution) which is a focal reducer instrument installed at the Nasmyth B focus of the telescope. We used the LR-R/LR-B grisms and a long-slit with a width between 1 arcsec and 1.5 arcsec, depending to the actual seeing conditions, oriented along the parallactic angle. For the data reduction, we have used the IRAF long-slit package. The spectra have been wavelength calibrated using Ar, Ne + Hg, Kr reference spectra. The flux calibration was obtained by observing a spectrophotometric standard.

In total, we observed all the 12 sources without a spectroscopic redshift. In 10 cases, the data were good enough to obtain a firm classification and redshift while for 2 sources the signal to noise is too low and they should be considered still unidentified.

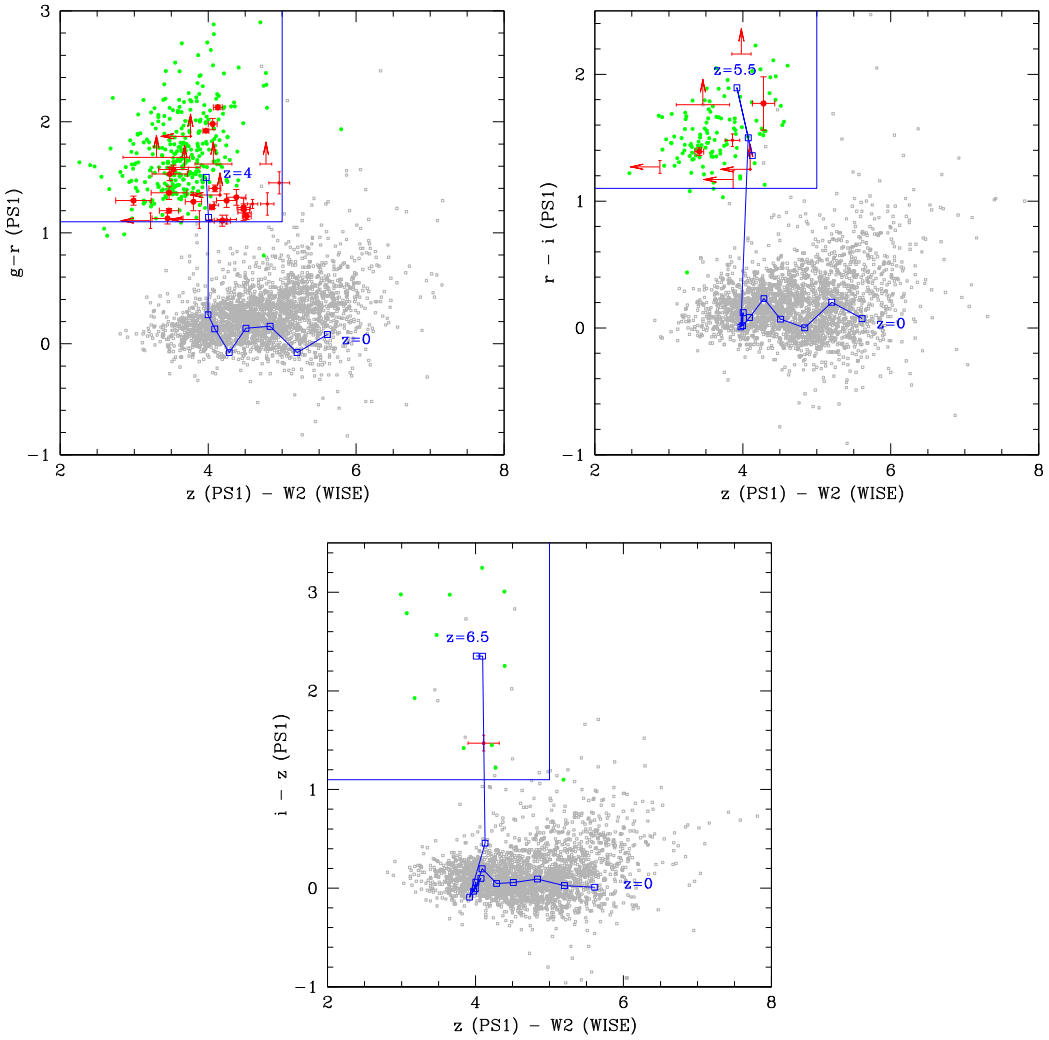

Figure 2. Diagnostic diagrams used to select $z > 4$ candidates from CLASS. We plot three different PS1 colours ($g-r$, $r-i$, and $i-z$) versus mid-IR colours ($z-$W2), computed between PS1 z filter and W2 filter of WISE at 4.6 micron (note that magnitudes from PS1 are in AB systems while W2 magnitudes are in Vega system). Red points are the CLASS objects that fulfill the selection criteria. Grey points show all the CLASS sources with a star-like PS1 counterpart and detected in WISE. Green points are the high-z quasars from the literature (including radio-quiet ones). In particular, they are quasars at $4<z<4.5$, at $4.6<z<5.5$, and at $5.6<z<6.5$, respectively, in the three panels. For clarity, errorbars are plotted only for the selected high-z candidates. For reference, we also plot the paths (blue lines) of the QSO template from Polletta et al. (2007) for redshifts ranging from 0 up to the maximum values indicated in each panel by steps of 0.5. The template has been absorbed for the neutral hydrogen scattering in the inter-galactic medium along the line of sight at $z = 4$, 4.5, and 5, respectively, in the three panels, using the transmission curve from Songaila (2004). Finally, the blue boxes indicate the regions used to select the candidates.

In nearly all cases, the sources are confirmed high-z AGN ($z > 3$) although not all have a redshift above the adopted threshold ($z = 4$). In one case (GB6J010135 + 153845), instead, the redshift is significantly lower than expected ($z = 1.5$). This was the only i-dropout candidate for which we predicted a very high redshift ($z \sim 5.5$–6.5). The optical spectrum, instead, shows a broad emission line at $\lambda = 7075$Å that can be identified as the Mg IIλ2798Å, leading to a redshift of 1.53. The continuum emission does not show any obvious dropout between the i and z band contrary to the value reported by the PS1 catalogue ($i-z = 1.47 \pm 0.07$ mag). Very likely this is a fake dropout due to some errors in the PS1 magnitudes.

Notably, with these observations we have found two new $z \geq 5$ AGN thus doubling the number of AGN in this redshift bin present in the CLASS sample. As described in Section 5, both objects have a radio spectrum that confirms their blazar nature. Therefore, they constitute a significant addition with respect to the total number of blazars at z above five discovered so far (four in total; see also Belladitta et al., in preparation). One source (GB6J164856 + 460341), in particular, has a redshift of 5.38 and it represents the second most distant blazar discovered so far (the highest being at $z = 5.47$, GB6J090631 + 693027; Romani et al. 2004).

We have not found, instead, high-redshift featureless blazars (i.e. BL Lac objects) even though our selection is potentially sensitive also to these objects. This lack of high-z BL Lac is likely due to their peculiar cosmological evolution (very weak or even negative; see e.g. Ajello et al. 2014 and references therein) that makes their detection at high redshifts very unlikely. In the following, with the term 'blazar' we will always indicate the QSO-like blazars (often called flat-spectrum radio quasar, FSRQ) due to the lack of featureless blazars at high redshifts.

In total, considering both the new identifications and those from the literature or from the SDSS, we have 20 QSO with $z \geq 4$ among the 37 candidates selected with the dropout method. Only two objects (5 per cent) are still unidentified. Six sources are in

Table 1. The list of dropout candidates selected from CLASS.

Name	CLASS	Redshift	Coordinates (J2000.0)	Mag (mag)	Dropout	Drop value (mag)	$z-$W2 (mag)	Ref.
GB6J001115 + 144608	QSO	4.96	00 11 15.24 + 14 46 01.8	18.28	*r*	1.39	3.41	(1)
GB6J001307 + 205335	QSO	3.53	00 13 11.10 + 20 53 42.7	17.79	*g*	1.11	4.02	LBT06/18
GB6J002121 + 155127	QSO	3.70	00 21 20.06 + 15 51 25.8	19.59	*g*	1.23	4.48	(1)
GB6J003126 + 150729	QSO	4.29	00 31 26.80 + 15 07 39.5	20.23	*g*	1.36	3.47	(1)
GB6J004348 + 342617	QSO	0.97	00 43 48.85 + 34 26 26.1	19.06	*g*	1.32	4.38	(10)
GB6J010135 + 153845	QSO	1.50	01 01 36.09 + 15 38 38.2	20.33	*i*	1.47	4.11	LBT11/17
GB6J012126 + 034646	QSO	4.13	01 21 26.15 + 03 47 06.7	18.77	*g*	1.25	4.08	LBT11/17
GB6J012202 + 030951	QSO	4.00	01 22 01.91 + 03 10 02.4	20.86	*g*	1.12	<3.88	(3)
GB6J012921 + 310303	QSO	3.56	01 29 21.85 + 31 02 58.5	19.26	*g*	1.20	3.47	(1)
GB6J024612 + 182334	QSO	3.59	02 46 11.82 + 18 23 30.1	19.22	*g*	1.15	4.52	(11)
GB6J040738 + 001713	QSO	3.70	04 07 36.61 + 00 17 26.3	19.60	*g*	1.26	4.60	TNG03/18
GB6J042423 + 144230	QSO	3.55	04 24 23.49 + 14 42 16.7	20.14	*g*	1.26	4.80	TNG03/18
GB6J061110 + 721814	–	–	06 11 09.17 + 72 18 15.6	19.78	*g*	1.45	4.96	LBT02/18
GB6J064057 + 671228	–	–	06 40 58.19 + 67 12 25.1	20.94	*r*	>1.76	3.46	TNG03/18
GB6J083548 + 182519	QSO	4.41	08 35 49.43 + 18 25 20.1	20.93	*g*	>1.87	<3.76	(1)
GB6J083945 + 511206	QSO	4.40	08 39 46.22 + 51 12 02.8	19.28	*g*	1.98	4.06	(1, 12)
GB6J090631 + 693027	QSO	5.47	09 06 30.75 + 69 30 30.8	20.54	*r*	>2.16	3.98	(5)
GB6J091825 + 063722	QSO	4.22	09 18 24.38 + 06 36 53.4	19.68	*g*	1.40	4.09	(1, 12)
GB6J100724 + 580201	QSO	3.77	10 07 24.88 + 58 02 03.5	17.59	*g*	1.23	4.05	(1)
GB6J102623 + 254255	QSO	5.28	10 26 23.62 + 25 42 59.4	20.06	*r*	1.77	4.28	(1, 12)
GB6J132512 + 112338	QSO	4.42	13 25 12.49 + 11 23 29.8	19.45	*g*	2.13	4.13	(1, 12)
GB6J134811 + 193520	QSO	4.40	13 48 11.26 + 19 35 23.5	20.64	*g*	1.53	3.48	(1)
GB6J141212 + 062408	QSO	4.47	14 12 09.97 + 06 24 06.8	20.19	*g*	1.29	2.99	(1, 12)
GB6J143023 + 420450	QSO	4.72	14 30 23.74 + 42 04 36.5	19.79	*r*	1.27	<2.88	(1)
GB6J143533 + 543605	QSO	3.81	14 35 33.78 + 54 35 59.3	20.20	*g*	1.13	3.45	(1)
GB6J151002 + 570256	QSO	4.31	15 10 02.93 + 57 02 43.4	20.52	*g*	1.21	4.48	(1, 12)
GB6J154929 + 170853	BL	1.2:	15 49 29.27 + 17 08 28.0	18.77	*g*	>4.03	3.80	(1)
GB6J155930 + 030444	QSO	3.89	15 59 30.98 + 03 04 48.3	20.12	*g*	1.29	4.25	(1)
GB6J161216 + 470311	QSO	4.36	16 12 16.76 + 47 02 53.6	20.53	*g*	1.28	3.80	(1)
GB6J162956 + 095959	QSO	5.00	16 29 57.28 + 10 00 23.5	20.77	*r*	1.17	<3.87	LBT05/18
GB6J164327 + 410359	QSO	3.86	16 43 26.24 + 41 03 43.5	20.05	*g*	1.11	4.19	(1)
GB6J164856 + 460341	QSO	5.36	16 48 54.53 + 46 03 27.4	20.31	*r*	1.48	3.86	LBT01/18
GB6J171103 + 383016	QSO	4.00	17 11 05.54 + 38 30 04.3	20.53	*g*	1.12	4.25	LBT01/18
GB6J205332 + 010307	QSO	3.59	20 53 31.73 + 01 03 42.2	19.72	*g*	1.18	4.49	TNG05/18
GB6J223927 + 225959	QSO	2.93	22 39 27.69 + 23 00 18.1	18.17	*g*	1.92	3.97	(1)
GB6J231449 + 020146	QSO	4.11	23 14 48.71 + 02 01 51.1	19.64	*g*	1.57	3.53	(8)
GB6J235758 + 140205	QSO	4.35	23 57 58.56 + 14 02 01.9	20.40	*g*	1.11	<3.22	LBT07/18

Note. **Column 1**: name; **column 2**: CLASS (QSO=broad emission line AGN; BL = BL Lac object); **column 3**: redshift (':' = tentative redshift); **column 4**: radio (8.4 GHz, VLA-A array) position (J2000.0) **column 5**: PS1 magnitude in the reddest filter of the dropout (i.e. *r* filter for *g*-dropout sources, *i* filter for *r*-dropout sources, *z* filter for *i*-dropout sources; **column 6**: type of dropout; **column 7**: dropout value; **column 8**: $z-$W2; **column 9**: reference for the optical spectrum (or to the spectroscopic identification): (1)=SDSS DR12, (2) = Stern et al. (2000), (3) = Sowards-Emmerd, Romani & Michelson (2003), (4) = Amirkhanyan & Mikhailov (2006), (5) = Romani et al. (2004), (6) = Healey et al. (2008), (7) = Hook & McMahon (1998), (8) = Hook et al. (2002); (9) = Hewett & Wild (2010); (10) = Ackermann et al. (2011); (11)=BZCAT; (12) = Sbarrato et al. (2013). Please note that some of the objects with an SDSS spectrum have been already published in the literature.

common with the sample of high-*z* blazar candidates selected by Sbarrato et al. (2013).

All the optical spectra of the $z \geq 4$ objects observed at LBT and TNG or with an optical spectrum from SDSS are reported in Fig. 3. A detailed analysis of these data is in progress. In particular, we are measuring the line widths and luminosities of the most important emission lines, like Ly α, C IVλ1549Å and CIII]λ1909Å (when observed) with the final goal of obtaining a reliable estimate of the mass of central SMBH and of the accretion rate.

The redshift distribution of all the $z \geq 4$ objects in CLASS is reported in Fig. 4.

4 COMPLETENESS OF THE SAMPLE

As described in the previous section, the identification level of the sample is very high (95 per cent). It is possible, however, that some high-*z* objects are missed by our selection. To check the completeness of our sample we have searched through the literature and in the SDSS spectroscopic database for high-*z* AGN among all the 11 000 CLASS sources, independently from their photometric colour, magnitude, or sky position. We found six additional $z > 4$ QSO (see Table 2). Two of them were not selected because they have a low Galactic latitude ($|b^{II}| < 20$ deg) while other three objects have a magnitude fainter than the adopted limit.[3] Only one source

[3]One of the objects (GB6J160608 + 312504) presents also a large optical-to-radio offset (1.22 arcsec), significantly larger than typical radio (and optical) error uncertainty. In addition, an optical spectrum of this source is not available in the literature and in the CGRaBS catalogue (Healey et al. 2008) the redshift is given as uncertain. We therefore consider this identification unreliable.

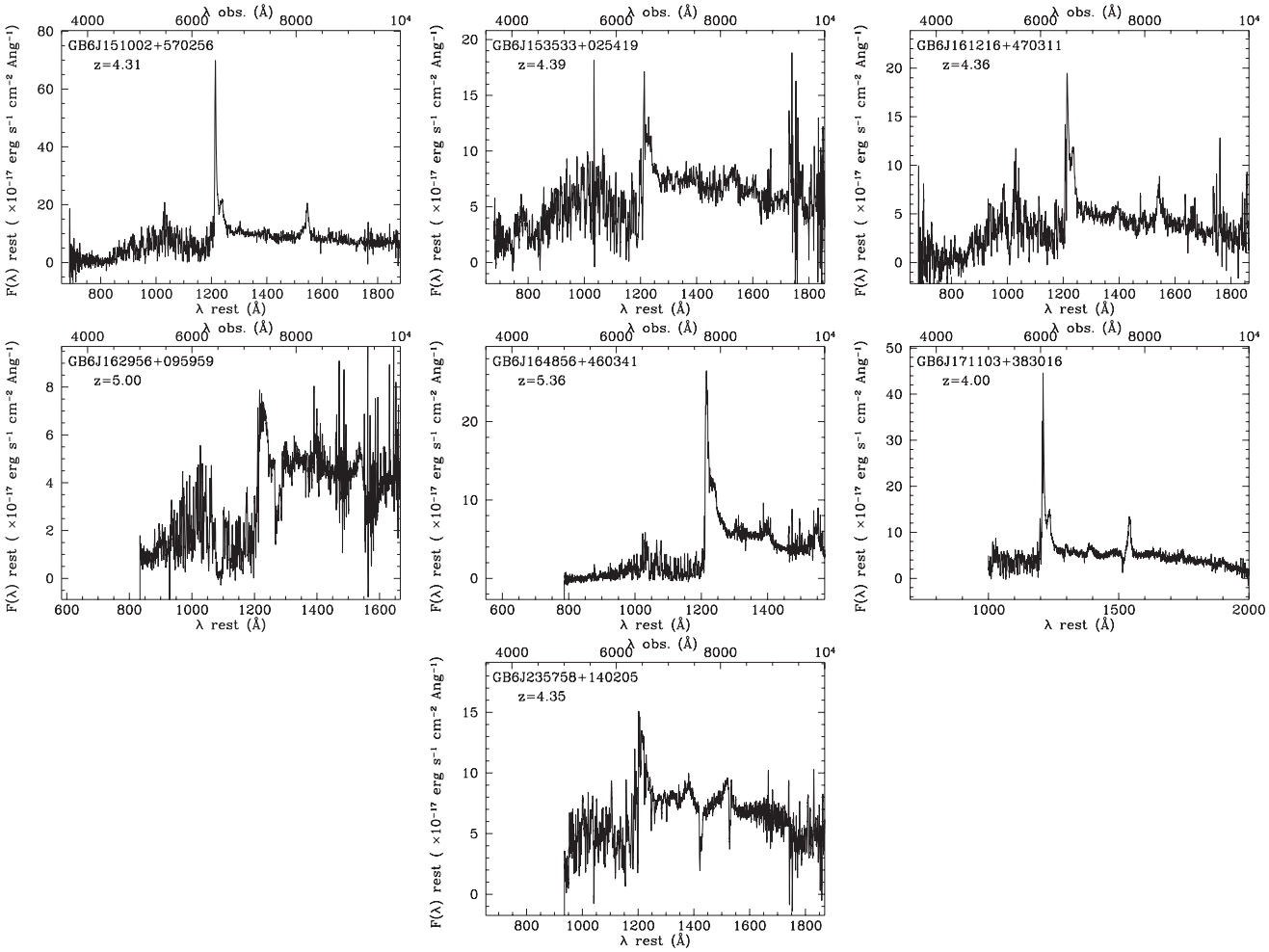

Figure 3. Optical spectra (either from SDSS or taken by our own observations) of 19 out of the 26 $z \geq 4$ QSO present in the CLASS survey (see the text for details).

(GB6J153533 + 025419) is not recovered because it does not show a significant dropout ($g-r = 0.79 \pm 0.07$) and, therefore, it can be considered as missed from our selection.[4] This confirms that our selection method is highly complete for $z > 4$ since it recovers nearly all (13/14) the already known high-z AGN in the sample. We note, instead, that for slightly lower values of redshift, the completeness level drops significantly: in Fig. 5 we show the fraction of high-z AGN (with mag < 21) from the literature or from SDSS DR12 that are present in CLASS (and in the sky area considered for the complete sample) and that are correctly recovered by our selection. While most (95 per cent) of the $z > 4$ objects are recovered, for redshifts below 4 this fraction decreases significantly, being around 25 per cent for $3.6 < z < 4$ and below 5 per cent for $3 < z < 3.6$.

We define as *complete sample*, the one defined at high Galactic latitude ($|b^{II}| > 20$ deg) and at a magnitude limit of 21 (in r, i, or z filter depending on the redshift of the source, as described in Section 2). This sample is composed by the 20 $z \geq 4$ of Table 1 plus the additional object (GB6J153533 + 025419) present in Table 2.

[4]In the SDSS, this source has a higher dropout value ($g-r = 1.18$) that would have allowed its inclusion in the sample. This suggests that the low dropout value observed in PS1 can be related to some photometric problem in PanSTARRS.

4.1 Impact of variability on the sample completeness

Blazars are variable sources. Variability can potentially affect the completeness of the CLASS sample which was built using non-simultaneous radio data. Variability can in fact make an intrinsically flat spectrum variable source to appear as a non-flat spectrum object depending on when fluxes have been measured in relation to the activity phase.

In order to estimate the importance of variability at radio frequencies, we have first compared the flux densities at 1.4 GHz computed in the NVSS and in the Faint Images of the Radio Sky at Twenty-cm (FIRST; Becker, White & Helfand 1995) surveys that have been carried out at different epochs. Since all CLASS objects at $z > 4$ are compact at both FIRST and NVSS resolution, any observed difference in the flux densities can be attributed to source variability and not to the different instrumental resolutions. From this comparison, we have estimated an rms flux variability of 14 per cent. We then used numerical simulations to evaluate the impact of this variability on the final completeness of the sample. Assuming a flat distribution of radio spectral indices between -0.5 and $+0.5$, we found that about 6 per cent of intrinsically flat-spectrum sources could have been missed due to variability, i.e. 1–2 objects. Using a Gaussian distribution of the spectral indices centred at $\alpha = 0$ would produce an even smaller percentage of missing sources due to variability.

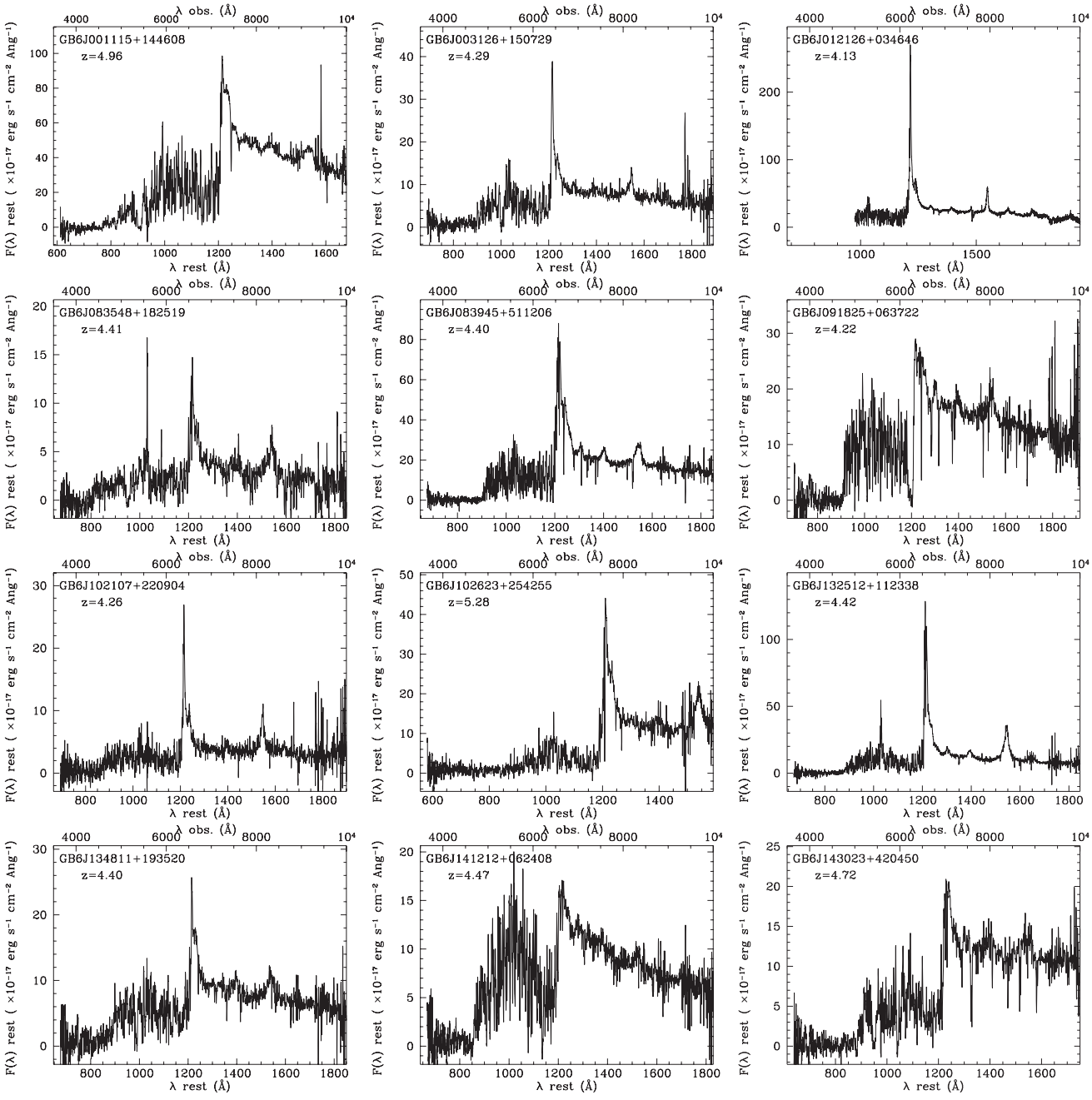

Figure 3 – *continued*

An independent way to estimate this effect is to use the flux densities available at other frequencies for the CLASS sources to derive independent estimates of the (non-simultaneous) spectral indices and to count the fraction of sources with $\alpha > 0.5$. Using the spectral indices between 150 MHz and 1.4 GHz, described in Section 5.1, we have one object with $\alpha > 0.5$ (see Fig. 6). Using, instead, the indices between 1.4 and 8.4 GHz, we have two sources (among the confirmed blazars, see discussion in the next section) with $\alpha > 0.5$. This is fully consistent with the results of our simulations. Even if small, we will consider the impact of this potential incompleteness on the derivation of the space densities that will be presented in Section 6.

Variability could, in principle, have an impact also on the optical selection of the high-z candidates since different levels of non-thermal radiation from the beamed jet can modify the optical colours of the source. However, unlike featureless blazars, FSRQ typically have most of the UV/optical emission produced by the accretion disc/broad line region while the emission from the relativistic jet is relatively less important at these wavelengths. This seems to be particularly true for high-z blazars, as discussed, for instance by Ghisellini et al. (2010). Therefore, we expect that variability in the optical band has an even lower impact on the completeness of the CLASS sample compared to that at radio wavelengths.

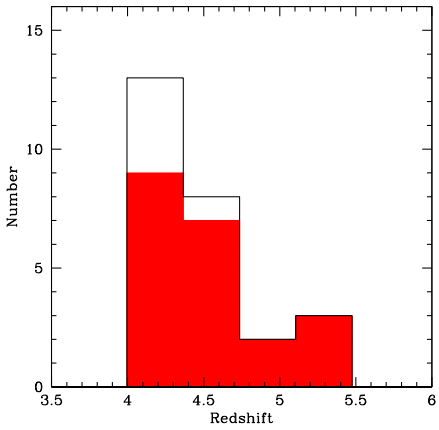

Figure 4. Redshift distribution of all the 26 $z > 4$ QSO present in the CLASS survey. The shaded area represents only those objects in the complete sample (see the text for details).

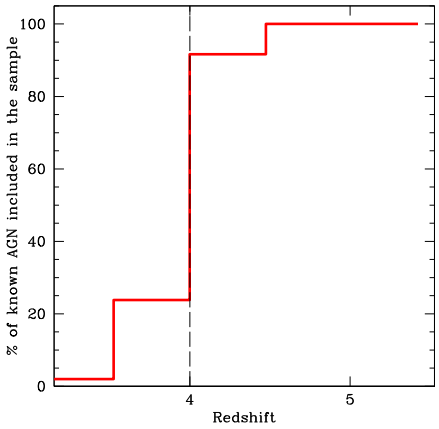

Figure 5. Fraction of know radio-loud AGN (from the literature or from the SDSS) that are recovered by our selection versus redshift. We are considering only the objects that fall in the area of sky that has been used to define the CLASS sample.

5 RADIO SPECTRAL SHAPES: GPS VERSUS FLAT-SPECTRUM SOURCES

By definition, CLASS contains sources with a flat radio spectrum between 1.4 and 5 GHz (observed frame). For this reason, CLASS should preferentially select blazars although sources that do not have a genuinely flat spectrum across the entire radio band could be also included.

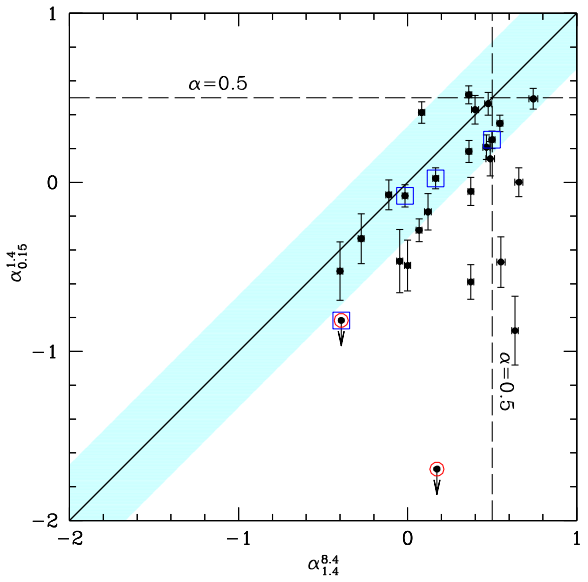

Figure 6. Radio spectral indices between 150 MHz and 1.4 GHz versus spectral indices between 1.4 GHz and 8.4 GHz of the AGN in CLASS with $z > 4$ (from Tables 1 and 2). Arrows indicate upper limits on $\alpha^{1.4}_{0.15}$ (i.e. sources not detected in the TGSS at 150 MHz). The boxes mark the objects already confirmed as blazars in the literature while the red open circles mark the sources (GB6J090631+693027, GB6J160608 + 312504) classified as peaked radio spectrum by Coppejans et al. (2017). The continuous line is the 1:1 relation while the light blue shaded area indicates the expected spread (90 per cent confidence level) due to variability (see the text for details).

The main contamination is that from AGN whose radio spectrum peaks at high frequencies. These objects, usually called Giga-Hertz Peaked Spectrum (GPS) sources (O'Dea 1998), appear compact at arcsecond resolution and with an apparent flat radio spectrum simply because we are observing the self-absorbed part of the radio spectrum. These are intrinsically small radio sources, possibly because of their young age. Interestingly, radio-loud AGN at high redshift often show these characteristics (Frey et al. 2003, 2005; Coppejans et al. 2016; Coppejans et al. 2017). At m.a.s. scales the emission is usually resolved, often showing a Compact-Symmetric Objects (CSO) morphology, i.e. a small-scale version of a radio galaxy with lobes, hot-spots, jets, and relatively weak cores. This is an indication that the relativistic jet is mis-aligned with respect to the observer. Examples are J2102 + 6015, at $z = 4.57$ (Frey et al. 2018), J1606 + 3124, at $z = 4.56$ (Coppejans et al. 2017), and J1427 + 3312, at $z = 6.12$ (Frey et al. 2008, Coppejans et al. 2016). It is important to note, however, that this is not always

Table 2. Other $z > 4$ QSO present in the CLASS survey.

Name	Redshift	Coordinates (J2000.0)	Mag (mag)	Dropout	Drop value (mag)	z−W2 (mag)	Ref.	b^{II} (deg)
GB6J025758 + 433837	4.07	02 57 59.08 + 43 38 37.7	19.86	g	1.04	3.25	(4)	−13.5101
GB6J102107 + 220904	4.26	10 21 07.58 + 22 09 21.6	21.46	g	>1.34	<4.16	(1)	55.6110
GB6J153533 + 025419	4.39	15 35 33.88 + 02 54 23.4	20.72	g	0.79	3.33	(1)	43.9170
GB6J160608 + 312504	4.56	16 06 08.52 + 31 24 46.5	21.32	r	>1.38	5.57	(6)	47.6632
GB6J171521 + 214547	4.01	17 15 21.25 + 21 45 31.7	21.51	g	>1.29	–	(7)	30.3650
GB6J195135 + 013442	4.11	19 51 36.02 + 01 34 42.7	20.56	g	1.16	3.65	(6)	−12.6097

Note. This table includes other $z > 4$ QSO present in the CLASS survey that have not been selected mostly because they have a low Galactic latitude or because they have magnitude below the adopted limit. Only one object (in bold face) is missed by the selection because of a low dropout value. This should be considered as part of the CLASS sample of high-z blazar candidates since it falls in the sky area considered for the selection and it has a magnitude brighter than the limit. Table caption as in the previous table except for the last column that contains the Galactic latitude.

true: the source J0906 + 6930 at $z = 5.47$ shows a clearly peaked radio spectrum (Coppejans et al. 2017) with a turnover frequency of 6.4 GHz corresponding to 41.4 GHz in the source rest frame. At the same time, Very Long Baseline Interferometry (VLBI) data found evidence of Doppler boosting (Zhang et al. 2017, Frey et al. 2018), which was further supported by the study of radio variability (Liodakis et al. 2018) and of the SED (An & Romani 2018). These results suggest that J0906 + 6930 is a GPS source likely oriented towards the observer. Indeed, this is considered the highest redshift blazar discovered so far (Romani et al. 2004). Therefore, the simple observation of a peaked radio spectrum does not firmly exclude the presence of beaming.

In order to distinguish between truly flat spectrum sources from GPS it is important to extend the analysis of the radio spectrum at higher and lower frequencies to detect possible hints of spectral curvature. If a source is a GPS we expect that the radio spectrum, sampled in a broad range of frequencies, will not be well represented by a single power law. In this case, we expect that the two-point spectral index computed at very high frequencies would appear steeper than the one computed at lower frequencies (convex spectrum).

The analysis of the radio spectral shape of CLASS high-z sources is presented in the following section.

5.1 Low-frequency data from TGSS

In order to cover the widest range of frequency, we have used the recently released TGSS survey (TIFR GMRT Sky Survey; Intema et al. 2017), which is carried out at 150 MHz with the Giant Metrewave Radio Telescope (GMRT), and the high-frequency data at 8.4 GHz, taken at VLA in A-configuration, that are available for the CLASS objects. For the range of redshift considered here, the TGSS survey covers the source rest-frame frequency of 0.85 GHz (at the average redshift of the sample, $z = 4.5$) while the 1.4 and 8.4 GHz flux densities correspond, respectively, to 8 and 46 GHz. Therefore, a spectral index computed by combining TGSS data with flux densities at 1.4 GHz (from NVSS) gives us indications of the spectral slope between 0.85 and 8 GHz, i.e. in a range similar to that considered using NVSS and GB6 data for local sources. The indices computed between 1.4 and 8.4 GHz, instead, correspond to a high-frequency (8-46 GHz) range.

The current data release of TGSS (ADR1) covers 90 per cent of the sky (36 900 deg^2 at declination greater than −53deg) at an rms of 5 mJy beam^{-1} and with a resolution of 25 arcsec × 25 arcsec (in the Northern hemisphere). Out of the 26 high-z sources in the CLASS complete sample, 17 are present in the TGSS catalogue. For the remaining objects, we have analysed the TGSS images and looked for a detection at lower significance. We found a detection (at least 2σ) in seven out of the nine objects not included in the TGSS source catalogue. For the two undetected objects, we consider an upper limit of the 150 MHz flux density of 15 mJy $= (3\times\text{rms})$.

In Fig. 6, we show the spectral indices between 150 MHz and 1.4 GHz compared to the indices between 1.4 and 8.4 GHz. It is important to note that these spectral indices are computed using non-simultaneous data. Variability can affect the spectral classification into blazars and GPS-like objects as shown, for instance, by Orienti, Dallacasa & Stanghellini (2007). In Fig. 6, we plot the expected spread (90 per cent confidence level) on the 1:1 relation assuming an rms variability of 14 per cent, estimated in the previous section, and assuming that variability is similar at all frequencies. Sources that are distant from the shaded area have a spectrum that is likely not well represented by a single power law.

From Fig. 6, we see that 18 objects fall within the shaded area around the 1:1 relation (or they are consistent with it considering the error bars) thus suggesting that their spectrum is well represented by a flat power law in a wide range of frequencies (between 150 MHz up to 8.4 GHz) without significant curvatures.

In eight cases, instead, the $\alpha_{0.15}^{1.4}$ is significantly flatter than $\alpha_{1.4}^{8.4}$, typical of GPS-like sources (convex spectrum). The most striking one is GB6J160608 + 312504 whose limit on $\alpha_{0.15}^{1.4}$ is significantly different from the slope measured between 1.4 and 8.4 GHz. This object is known to have a spectrum peaking at 2.6 GHz (Coppejans et al. 2017), corresponding to 14.4 GHz in the source rest frame. VLBI observations suggest a Compact-Symmetric Objects (CSO) morphology (Coppejans et al. 2017). Another object that lies below the 1:1 relation in Fig. 6 is GB6J090631 + 693027, which, again, has been classified by Coppejans et al. (2017) as GPS (see the discussion above).

In Table 3, we report the radio spectral type ('Flat'/'Peaked') as derived from the analysis of Fig. 6.

In summary, 18 out of 26 high-z sources in CLASS (14 in the complete sample) have a spectral index between 0.15 and 1.4 GHz consistent with the index between 1.4 and 8.4 GHz (considering the possible variability), i.e. they have a genuine flat radio spectrum on a wide range of frequencies, between 150 MHz up to 8.4 GHz, corresponding to 0.83-46 GHz in the sources' rest frame (at the average redshift of the sample). This strongly supports the idea that these are beaming dominated objects and, therefore, likely observed at relatively small angles.

For the remaining objects, the situation is less clear since we have indications for a significant change of shape which may suggest a GPS nature. These sources could be mis-aligned AGN although we cannot completely exclude their blazar nature, as in the case of J0906+6930 (GB6J090631 + 693027).

It is interesting to compare these numbers with the ones discussed in Coppejans et al. (2017), who studied the radio spectral shapes of a sample of 30 high-z ($z > 4.5$) radio-loud AGN selected at 1.4 GHz. They grouped the sources into three classes: flat-spectrum (blazar) objects, steep-spectrum objects, and sources with a peaked radio spectrum. They found that the three classes are almost evenly populated. In CLASS, where the selection is made at higher frequencies (5 GHz) and where steep spectrum objects have been excluded by definition, we found that the majority (at least 69 per cent) of the objects are truly flat-spectrum objects over a wide range of frequencies. This result supports the strategy of using a 5 GHz selection, coupled to the constraint on the spectral slope between 1.4 and 5 GHz, to efficiently select a sample of high-z blazars. In contrast, in a radio selection carried out at lower frequencies (e.g. 1.4 GHz) and without any constraint on the radio slope, the blazar selection efficiency falls down to 30 per cent.

5.2 Low-frequency data from GLEAM

In the analysis presented in the previous section, we have inferred the radio spectral shapes on the basis of the comparison between the slopes computed between two frequencies. This approach was imposed by the limited amount of data points available for each object. In some cases, however, we can carry out a proper spectral analysis thanks to the availability of several (simultaneous) data points taken from the GaLactic and Extragalactic All-sky MWA (GLEAM) survey (Hurley-Walker et al. 2016). GLEAM is a low-frequency radio survey carried out with Murchison Widefield Array (MWA),

Table 3. Spectral radio properties.

Name	$S_{0.15\,\mathrm{GHz}}$ (mJy)	$S_{1.4\,\mathrm{GHz}}$ (mJy)	$S_{8.4\,\mathrm{GHz}}$ (mJy)	$\alpha_{0.15}^{1.4}$	$\alpha_{1.4}^{8.4}$	Spectral type
GB6J001115 + 144608	49	36	15	0.14	0.49	Flat:
GB6J003126 + 150729	13	42	86	−0.53	−0.40	Flat
GB6J012126 + 034646	11	78	25	−0.88	0.64	Peaked
GB6J012202 + 030951	84	99	121	−0.07	−0.11	Flat
GB6J025758 + 433837	79	149	132	−0.28	0.07	Flat:
GB6J083548 + 182519	84	53	23	0.21	0.47	Flat
GB6J083945 + 511206	15	43	16	−0.47	0.55	Peaked
GB6J090631 + 693027	–	93	188	<−0.82	−0.39	Peaked
GB6J091825 + 063722	21	31	25	−0.17	0.12	Flat
GB6J102107 + 220904	486	153	80	0.52	0.36	Flat
GB6J102623 + 254255	451	257	105	0.25	0.50	Flat
GB6J132512 + 112338	22	82	42	−0.59	0.37	Peaked
GB6J134811 + 193520	52	52	16	0.00	0.66	Peaked
GB6J141212 + 062408	123	47	23	0.43	0.40	Flat
GB6J143023 + 420450	177	211	217	−0.08	−0.02	Flat
GB6J151002 + 570256	213	202	150	0.02	0.17	Flat
GB6J153533 + 025419	146	58	50	0.41	0.08	Flat
GB6J160608 + 312504	–	663	486	<−1.70	0.17	Peaked
GB6J161216 + 470311	153	54	23	0.46	0.48	Flat
GB6J162956 + 095959	160	53	14	0.49	0.74	Flat
GB6J164856 + 460341	12	34	37	−0.47	−0.05	Flat:
GB6J171103 + 383016	15	45	45	−0.49	0.00	Peaked:
GB6J171521 + 214547	1177	540	203	0.35	0.55	Flat
GB6J195135 + 013442	47	99	162	−0.33	−0.27	Flat
GB6J231449 + 020146	111	125	64	−0.05	0.37	Peaked:
GB6J235758 + 140205	167	111	58	0.18	0.36	Flat

Note. **Column 1**: name (in bold face the sources belonging to the complete sample); **column 2**: flux density at 150 MHz from TGSS; **column 3**: flux density at 1.4 GHz from NVSS; **column 4**: flux density at 8.4 GHz from CLASS; **column 5**: spectral index between 150 MHz and 1.4 GHz; **column 6**: spectral index between 1.4 GHz and 8.4 GHz; **column 7**: spectral type. The symbol ':' indicates that radio spectral classification is uncertain.

the low-frequency Square Kilometre Array (SKA1 LOW) precursor located in Western Australia. The first release of the extragalactic catalogue covers the entire high Galactic latitude (>30°) sky south of +30° of declination (24 831 deg^2), excluding some areas such as the Magellanic Clouds. The catalogue contains flux density measurements in 20 separate intervals between 72 and 231 MHz with a flux density limit (90 per cent completeness) of 170 mJy. It should be noted, however, that the limited resolution (100 arcsec) of the telescope may affect the spectral analysis if strong, nearby sources are present.

In total, 7 CLASS high-z sources are currently detected in GLEAM, out of the 16 objects falling in the sky area covered by the survey. In Fig. 7, we show the wide band radio spectra, from 72 MHz up to 8.4 GHz, of these seven sources. In particular, we report the integrated flux densities from the GLEAM catalogue. We fitted all the photometric points with a simple power law to check the actual radio spectral slopes. Overall, the radio spectra computed on a wide range of frequencies are flat (α <0.5), confirming the classification previously derived using TGSS and high-frequency data. Only in one case (GB6J153533 + 025419), there are hints for a steepening at low frequencies (below 80–100 MHz, corresponding to 400–550 MHz in the sources' rest frame) probably indicating the presence of extended, non-beamed radio emission.

Overall, the spectral analysis of the few CLASS objects with data from GLEAM supports the results obtained in the previous section, based on few, non-simultaneous, data points giving us confidence on the reliability of our radio spectral classification.

6 SPACE DENSITY OF HIGH-REDSHIFT BLAZARS

Thanks to its completeness, the CLASS sample can be used to derive the space density of blazars above $z = 4$. In particular, we can compute the space density of blazars with a radio power at 5 GHz between 10^{27} and 1.3×10^{28} W Hz^{-1}, which is the observed range of luminosities. The complete sample contains 21 objects with redshift between 4 and 5.4. 14 have been classified as blazars, as discussed in the previous sections.[5] Since we cannot exclude that some of the remaining seven objects are blazars, we consider the total sample as an upper limit on the number of blazars. The CLASS survey covers 16 300 deg^2 of sky but we are now considering the complete sample that is defined for Galactic latitudes above 20 deg (see Section 7) corresponding to a sky area of 13 120 deg^2 (=4 steradians), i.e. 1/3 of the total sky area.

In order to compute the space density of high-z blazars, we use the method described, for instance, by Avni & Bahcall (1980): for each object with redshift between z_1 and z_2 we compute the volume of the Universe within which it could have been discovered as:

$$V_{\mathrm{obs}} = \frac{A}{4\pi} V_{\mathrm{max}},$$

where A is the sky area (in steradians) covered by the survey and V_{max} is the co-moving volume of Universe between z_1 and the minimum value among z_2, z^R_{max} and z^O_{max}. The quantities z^R_{max} and

[5]For consistency, we are not considering GB6J090631 + 693027 as blazar, given its peaked radio spectrum.

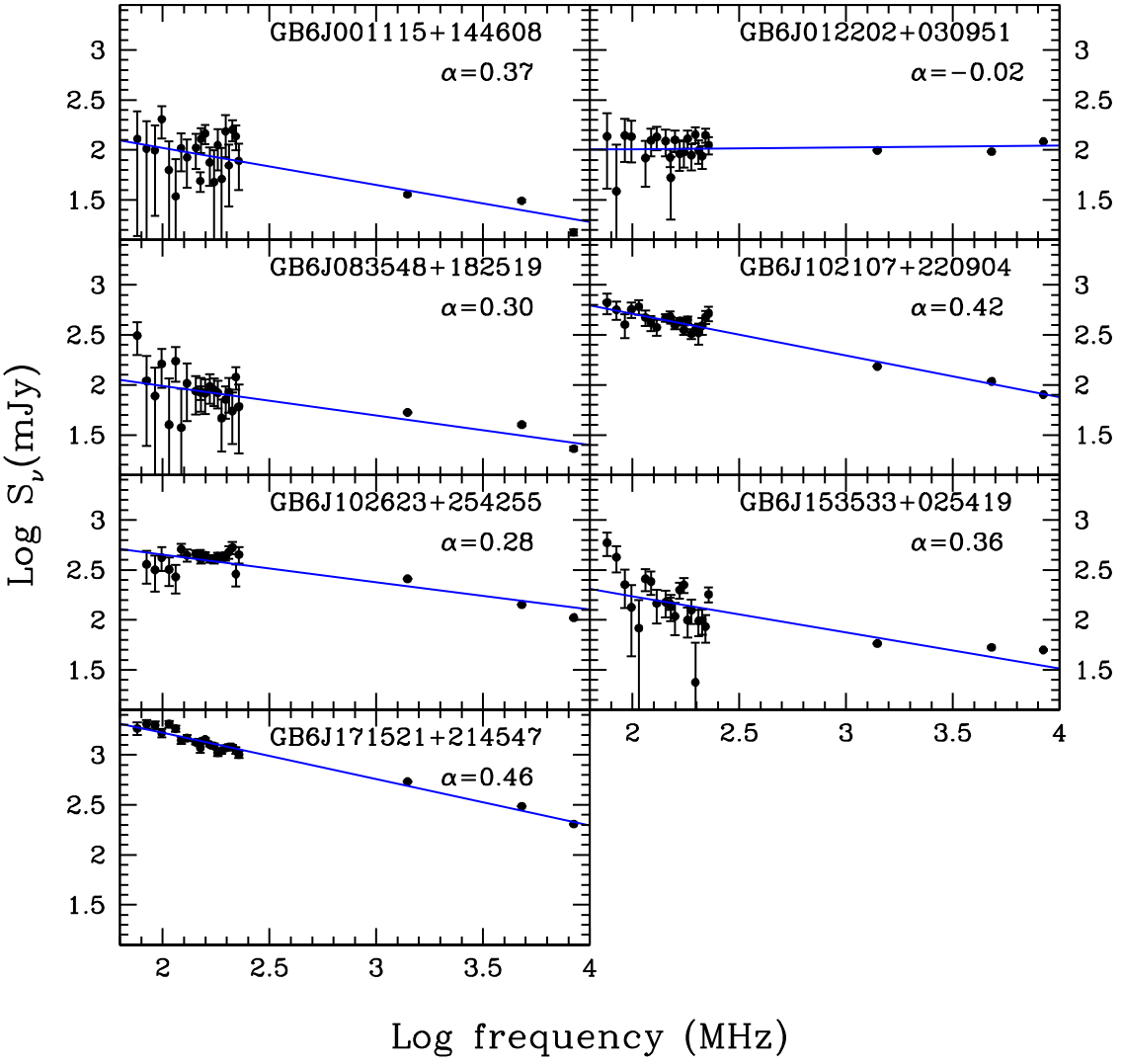

Figure 7. Radio spectra (observed frame) of the seven high-z from CLASS detected in the GLEAM survey.

$z^O_{\rm max}$ are, respectively, the redshift at which the observed flux from the source would be equal to the radio/optical flux limit of the survey. The reason for taking the minimum of the three values of redshift is that the $V_{\rm max}$ must be computed on the most stringent among the radio/optical constraints. If both values are larger than z_2 then the $V_{\rm max}$ is simply the co-moving volume of Universe between z_1 and z_2.

The space density then is:

$$\rho = \sum \frac{1}{V_{\rm obs}}$$

with an error that is given by:

$$\mathrm{err}_\rho = \frac{\mathrm{err}}{N}\rho,$$

where N is the observed number of blazars in the given redshift bin and err is the Poissonian uncertainty on N.

Using this method,[6] we compute a space density of blazars at redshift between 4 and 5.5 and with radio powers at 5 GHz between 10^{27} and 1.3×10^{28} W Hz^{-1} of $\rho_{\rm flat} = 0.13^{+0.05}_{-0.03}$ Gpc^{-3}. Considering all the objects of the sample the density is $\rho_{\rm all} = 0.17^{+0.05}_{-0.04}$ Gpc^{-3}. This is the first actual estimate of the blazar space density in this range of redshift.

As explained in the previous sections, there are two potential sources of incompleteness, one related to the lack of spectroscopic confirmation of two high-z candidates (see Section 3) and one due to variability (see Section 4.1). In particular, one of the two candidates still unclassified (GB6J064057 + 671228) is potentially interesting since it has a flat radio spectrum (including the flux density at 150 MHz) and it is an r-dropout source, i.e. likely at $z > 4.5$. The

[6]For the k-corrections, we have assumed an optical spectral index of 0.44 (Vanden Berk et al. 2001) and we used the radio spectral index computed between 150 MHz and 1.4GHz. We note that the assumption on the optical spectral index has a very little impact on the final results since we are considering a very limited rest-frame wavelength range. A variation of the optical spectral index of ±0.5 only produces a variation smaller than ±0.04 dex on the computed space densities

other one (GB6J061110 + 721814), instead, is a *g* dropout (i.e. with redshift between 3.5 and 4.5) and with a possibly peaked radio spectrum. If we take these objects as true high-z sources, and if we consider also the possible fraction of missing objects due to variability, we obtain marginally higher space densities ($\rho_{\rm flat} = 0.15$ Gpc^{-3} and $\rho_{\rm all} = 0.19$ Gpc^{-3}).

7 DISCUSSION

It is now interesting to compare the space densities computed in the previous section with the predictions based on the radio selected sample of FSRQ recently published by Mao et al. (2017) (hereafter M17). The sample is based on the combination of FIRST and GB6 surveys and it has a relatively high radio flux limit (220 mJy) and covers 9500 deg^2 of sky. Given the large flux limit, this sample mostly contains objects with redshift below 4, with only one source at redshift above 4 (GB6J102623 + 254255, $z = 5.28$). Based on these data, M17 have found that the best parametrization for the cosmological evolution of FSRQ is a luminosity-dependent density evolution (LDDE) where the space density of FSRQ peaks at a redshift that depends on the luminosity of the object, being higher for the objects with higher radio luminosities. The radio luminosity function, instead, is well represented by a double power-law function. We used the analytical form presented in M17 to derive the expected space density as a function of redshift of the FSRQ in the same luminosity range of the high-z objects in CLASS. Since M17 defined their sample at 1.4 GHz, we compute the range of radio luminosities of CLASS high-z objects at this frequency i.e. log $L_{1.4\,\rm GHz}$ = log ($P_{1.4\rm GHz} \times \nu_{1.4\rm GHz}$)= 43.04–44.43 erg s^{-1}. We then integrated the radio luminosity function of M17 in this range of luminosities using the best-fitting LDDE evolution. The result is reported in Fig. 8 together with the densities computed using the CLASS complete sample in two bins of redshifts. We also added the upper limit between $z = 5.5$ and $z = 6$ based on the fact that the none of the candidates in this range of redshift (i.e. the objects with a dropout in the *i* band) turned out to be true high-z objects.

The CLASS data points follow the predictions of M17 that are based on sources with redshift much lower than the ones of the CLASS objects. Even considering the missing identification in CLASS (GB6J064057 + 671228), which could be a $z > 4.5$ blazar, the densities computed with the CLASS sample are still consistent with the predictions of M17.

According to this modelization, the peak of the space density, in this luminosity bin, is at $z \sim 2$, a value similar to that found for the radio-quiet QSO (e.g. Hopkins, Richards & Hernquist 2006). This is significantly different from the evolution estimated by Ajello et al. (2009) using an X-ray selected sample of blazars derived from the Swift–BAT survey that shows a peak at much higher redshifts $z \sim 4$ (Ajello et al. 2009). The difference cannot be ascribed to a different redshift sensitivity of the two samples since the redshift interval of the objects used by Ajello et al. (2009) is similar to that of the FSRQ considered by M17.

To further evaluate the position of the peak in the space density distribution in this range of radio luminosity, we have considered the QSO in CLASS with a redshift of 3. At this redshift all the QSO with a radio luminosity in the considered range, have a flux density above the limit of 30 mJy and, therefore, they are expected to be included in the sample. We consider the sky area covered by the SDSS to maximize the number of identifications. In this area (28 per cent of the total sky), the number of QSO in CLASS with z between 3 and 3.2 and a (log) radio luminosity at 1.4 GHz between 43.04 and 44.43 erg s^{-1} is 38 corresponding to a space density of

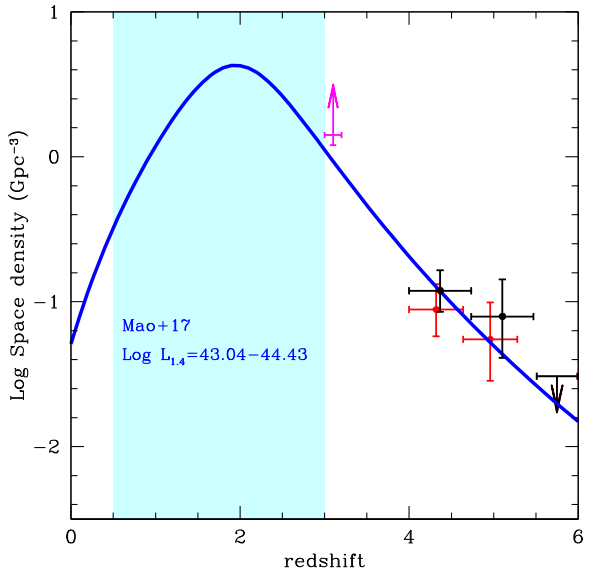

Figure 8. Space density versus redshift of the blazar candidates in CLASS considering all the 21 objects in the complete sample (black point) or just those with a flat radio spectrum in a wide range of frequencies (14 objects, red points). The blue solid line represents the expected densities computed by integrating the best-fitting radio luminosity function of M17 in the same range of radio luminosities (at 1.4 GHz) observed in the CLASS high-z sample and using the LDDE cosmological evolution found by M17 (clean sample). The shaded area indicates the range of redshift actually sampled by the FSRQ studied by M17 in the indicated range of radio luminosity. The magenta arrow represents the lower limit on the space density derived from CLASS at $z \sim 3$ (see the text for details).

1.4 Gpc^{-3}. This is a lower limit since the identification level of CLASS, even considering the area covered by SDSS, is relatively low (15 per cent). However, we expect that most of the QSO in this redshift range have been already identified, at least down to the magnitude limit of SDSS, thanks to the dedicated searches carried out in the past using the dropout method (in this case, the dropout falls in the *u* band; Fan et al. 1999). In any case, the lower limit (see Fig. 8) is clearly much higher than the 2 points at $z > 4$ thus excluding the hypothesis of a peak at $z \sim 4$.

The observed discrepancy between the results based on radio selected samples and those from the BAT survey needs to be investigated. In the context of a luminosity-dependent density evolution, the observed differences could be explained if the blazars selected by BAT were systematically more luminous (in the radio band) than those selected by M17 or in the CLASS survey. Indeed, about 80 per cent of the blazars in the BAT sample with $z > 2$ (i.e. those that allow to constrain the peak of the evolution) have a radio luminosity above 10^{44} erg s^{-1} while only 14 per cent of the CLASS high-z objects in the complete sample have a radio luminosity in this range. It is thus possible that the space density of blazars with the highest radio luminosities, above the range observed in CLASS, peaks at larger redshift than observed at lower luminosities. If confirmed, this would imply that only the most luminous radio-loud QSO have a cosmological evolution that peaks at very high redshifts (4) the majority having an evolutionary behaviour very similar to that observed in radio-quiet QSO, peaking at $z \sim 2$.

Another possibility is that radio and X-ray selections are sampling different classes of objects having different cosmological behaviours. This is not unusual within the blazar family: BL Lac objects are known to show significantly different cosmological

evolution depending on the selection band, being weakly positive in radio selections (Stickel et al. 1991; Marcha & Caccianiga 2013), negative in X-ray selections (e.g. Morris et al. 1991; Rector et al. 2000; Beckmann et al. 2003) and showing little or no evolution when mixed (radio plus X-rays) selections are used (e.g. Caccianiga et al. 2002). One of the discussed possibilities is that the two selections are sampling different sub-populations of BL Lacs (the so-called High-Energy peaked BL Lac and Low-Energy peaked BL Lac) that evolve in a different way with cosmic time. A similar difference could be present also among the class of FSRQ: in this case, X-rays (BAT) and radio surveys may be sampling different sub-populations of FSRQ having different X-ray to radio luminosity ratios and different cosmological evolutions. A systematic study of the X-ray properties of all the high-z CLASS objects is in progress in order to establish the difference/similarities between this sample and the blazars selected in the X-rays at lower redshifts (see Ighina et al. 2018 for first results of this analysis).

8 SUMMARY AND CONCLUSIONS

We have presented a well-defined, radio flux limited sample of 26 high-z (>4) blazar candidates selected from CLASS, which is a survey of flat-spectrum radio sources (between 1.4 and 5 GHz). In particular, 21 objects constitute a statistically complete sample down to a magnitude of 21, thanks to dedicated spectroscopic follow-ups at LBT and TNG. Notably, these observations have provided two new $z \geq 5$ objects that represent a significant increase of the number of blazars above $z = 5$ currently known (four objects found to date).

By studying the radio spectrum over a wide range of frequencies (from 150 MHz to 8.4 GHz, corresponding to 0.85-46 GHz in the rest frame of the sources), we found that more than half (18 sources) of the CLASS objects are genuine flat-spectrum sources, the remaining fraction being likely represented by GPS-like objects. Considering the complete sample, the number of truly flat spectrum sources is 14. We cannot exclude, however, that some of the objects with a GPS-like radio spectrum could be blazars. High-resolution radio data (VLBI) and/or variability studies are needed in order to establish their blazar/non-blazar nature on a firm basis. We have an approved program at the European VLBI Network (EVN) to carry out a complete follow up at 5 GHz all the high-z sources in CLASS.

We then used the complete sample to compute the space density of blazars at redshift between 4 and 5.5. We found a value of $0.13^{+0.05}_{-0.03}$ Gpc^{-3}, considering only the confirmed blazars, and $0.17^{+0.05}_{-0.04}$ Gpc^{-3}, using the entire sample. Accounting for the possible incompleteness, the values of densities become $\rho_{\rm flat} = 0.15$ Gpc^{-3} and $\rho_{\rm all} = 0.19$ Gpc^{-3}, respectively. This is the first estimate (not a lower limit or an extrapolation) of the space density of blazars in this redshift interval.

The resulting space densities are in good agreement with the predictions recently presented by M17 using a sample of FSRQ with $z < 4$. According to these authors, the evolution of FSRQ of these luminosities should peak at a redshift 2, which is similar to what is observed in radio-quiet QSO but significantly different from what has been found by Ajello et al. (2009) using an X-ray selected sample of blazars. The origin of this difference is not clear and it may suggest that only the most luminous radio-loud QSO present a peak of the space density at very high redshift, while the bulk of the population has a cosmological evolution more similar to radio-quiet QSO.

ACKNOWLEDGEMENTS

We thank I.W. Browne for useful discussions and the referee for his/her comments that improved the quality of the paper. This work is based on observations made with the Large Binocular Telescope (LBT, program IT-2017B-006) and the Telescopio Nazionale Galileo (TNG, programs A36TAC25 and A37TAC5). In an early stage of the project, this work has also used data from the William Herschel Telescope (WHT, program SW2015a48) and the Apache Point Observatory 3.5-meter Telescope. LBT is an international collaboration among institutions in the United States of America, Italy, and Germany. The LBT Corporation partners are the University of Arizona on behalf of the Arizona university system and the Istituto Nazionale di Astrofisica. TNG is operated on the island of La Palma by the Fundación Galileo Galilei of the INAF (Istituto Nazionale di Astrofisica) at the Spanish Observatorio del Roque de los Muchachos of the Instituto de Astrofisica de Canarias WHT is operated on the island of La Palma by the Isaac Newton Group (ING). APO 3.5-meter telescope is owned and operated by the Astrophysical Research Consortium. This work is based on SDSS data. Funding for the Sloan Digital Sky Survey IV has been provided by the Alfred P. Sloan Foundation, the U.S. Department of Energy Office of Science, and the Participating Institutions. SDSS-IV acknowledges support and resources from the Center for High-Performance Computing at the University of Utah. The SDSS website is www.sdss.org. This publication makes use of data products from the Wide-field Infrared Survey Explorer, which is a joint project of the University of California, Los Angeles, and the Jet Propulsion Laboratory/California Institute of Technology, funded by the National Aeronautics and Space Administration. We thank the staff of the GMRT that made these observations possible. GMRT is run by the National Centre for Radio Astrophysics of the Tata Institute of Fundamental Research. AC, AM, SB, RDC, PS acknowledge support from ASI under contracts ASI-INAF no. I/037/12/0 and no. 2017-14-H.0 and from INAF under PRIN SKA/CTA FORECaST. CC acknowledges funding from the European Union's Horizon 2020 research and innovation programme under the Marie Sklodowska-Curie grant agreement No 664931 SA acknowledges support from CIDMA strategic project (UID/MAT/04106/2013), ENGAGE SKA (POCI-01-0145-FEDER-022217), funded by COMPETE 2020 and FCT, Portugal.

REFERENCES

Ackermann M. et al., 2011, ApJ, 743, 171
Ajello M. et al., 2009, ApJ, 699, 603
Ajello M. et al., 2014, ApJ, 780, 73
Amirkhanyan V. R., Mikhailov V. P., 2006, Astrophysics, 49, 184
An H., Romani R. W., 2018, ApJ, 856, 105
Avni Y., Bahcall J. N., 1980, ApJ, 235, 694
Becker R. H., White R. L., Helfand D. J., 1995, ApJ, 450, 559
Beckmann V., Engels D., Bade N., Wucknitz O., 2003, A&A, 401, 927
Browne I. W. A. et al., 2003, MNRAS, 341, 13
Caccianiga A., Maccacaro T., Wolter A., Della Ceca R., Gioia I. M., 2002, ApJ, 566, 181
Carnall A. C. et al., 2015, MNRAS, 451, 16
Chambers K. C. et al., 2016, preprint (arXiv:1612.05560)
Condon J. J., Cotton W. D., Greisen E. W., Yin Q. F., Perley R. A., Taylor G. B., Broderick J. J., 1998, AJ, 115, 1693
Coppejans R. et al., 2016, MNRAS, 463, 3260
Coppejans R. et al., 2017, MNRAS, 467, 2039
Fan X. et al., 1999, AJ, 118, 1
Fan X. et al., 2000, AJ, 119, 1

Fan X. et al., 2003, AJ, 125, 1649
Frey S., Mosoni L., Paragi Z., Gurvits L. I., 2003, MNRAS, 343, L20
Frey S., Paragi Z., Mosoni L., Gurvits L. I., 2005, A&A, 436, L13
Frey S., Gurvits L. I., Paragi Z., Gabányi K. É., 2008, A&A, 484, L39
Frey S., Titov O., Melnikov A. E., de Vicente P., Shu F., 2018, A&A, 618, 68
Ghisellini G. et al., 2010, MNRAS, 405, 387
Ghisellini G., Sbarrato T., Tagliaferri G., Foschini L., Tavecchio F., Ghirlanda G., Braito V., Gehrels N., 2014, MNRAS, 440, 111
Ghisellini G., Haardt F., Ciardi B., Sbarrato T., Gallo E., Tavecchio F., Celotti A., 2015, MNRAS, 452, 345
Gregory P. C., Scott W. K., Douglas K., Condon J. J., 1996, ApJS, 103, 427
Healey S. E. et al., 2008, ApJS, 175, 97
Hewett P. C., Wild V., 2010, MNRAS, 405, 2302
Hook I. M., McMahon R. G., 1998, MNRAS, 294, L7
Hook I. M., McMahon R. G., Shaver P. A., Snellen I. A. G., 2002, A&A, 391, 509
Hopkins P. F., Richards G. T., Hernquist L., 2006, ApJ, 654, 731
Hurley-Walker N. et al., 2016, MNRAS, 464, 1146
Ighina L. et al., 2018, Contribution to the 13th Italian meeting on AGN, Milan Oct 2018, Zenodo. Available at: http://doi.org/10.5281/zenodo.1475236
Intema H. T., Jagannathan P., Mooley K. P., Frail D. A., 2017, A&A, 598, 78
Liodakis I., Hovatta T., Huppenkothen D., Kiehlmann S., Max-Moerbeck W., Readhead A. C. S., 2018, ApJ, 866, 137
Mao P., Urry C. M., Marchesini E., Landoni M., Massaro F., Ajello M., 2017, ApJ, 842, 87
Marcha M. J., Caccianiga A., 2013, MNRAS, 430, 2464
McGreer I. D., Becker R. H., Helfand D. J., White R. L., 2006, ApJ, 652, 157
Merloni A., 2016, in Lecture Notes in Physics, Vol. 905, Astrophysical Black Holes. Springer-Verlag, Berlin, p. 101
Morris S. L., Stocke J. T., Gioia I. M., Schild R. E., Wolter A., Maccacaro T., della Ceca R., 1991, ApJ, 380, 49
Myers S. T. et al., 2003, MNRAS, 341, 1
Norris R. P. et al., 2011, PASP, 28, 215
O'Dea C. P., 1998, PASP, 110, 493
Orienti M., Dallacasa D., Stanghellini C., 2007, A&A, 475, 813
Polletta M. et al., 2007, ApJ, 663, 81
Rector T. A., Stocke J. T., Perlman E. S., Morris S. L., Gioia I. M., 2000, ApJ, 120, 1626
Romani R. W., Sowards-Emmerd D., Greenhill L., Michelson P., 2004, ApJ, 610, L9
Sbarrato T., Ghisellini G., Nardini M., Tagliaferri G., Greiner J., Rau A., Schady P., 2013, MNRAS, 433, 2182
Sbarrato T., Ghisellini G., Tagliaferri G., Foschini L., Nardini M., Tavecchio F., Gehrels N., 2015, MNRAS, 446, 2483
Snellen I., McMahon R., Dennett-Thorpe J., Jackson N., Mack K.-H., Xanthopoulos E., 2001, MNRAS, 325, 1167
Songaila A., 2004, AJ, 2598
Sowards-Emmerd D., Romani R. W., Michelson P. F., 2003, ApJ, 590, 109
Pogge R. W. , et al., 2010, Proc. SPIE, 7735, 77350A
Stern D., Djorgovski S. G., Perley R. A., de Carvalho R. R., Wall J. V., 2000, AJ, 119, 1526
Stickel M., Fried J. W., Kuehr H., Padovani P., Urry C. M., 1991, ApJ, 374, 431
Urry C. M., Padovani P., 1995, PASP, 107, 803
Valiante R., Agarwal B., Habouzit M., Pezzulli E., 2017, PASA, 34, 31
Vanden Berk D. E. et al., 2001, AJ, 122, 549
Vito F. et al., 2018, MNRAS, 473, 2378
Volonteri M., 2010, A&AR, 18, 279
Volonteri M., Haardt F., Ghisellini G., Ceca R. D., 2011, MNRAS, 416, 216
Wright E. L. et al., 2010, AJ, 140, 1868
Wu J., Ghisellini G., Hodges-Kluck E., Gallo E., Ciardi B., Haardt F., Sbarrato T., Tavecchio F., 2017, MNRAS, 468, 109
Zeimann G. R., White R. L., Becker R. H., Hodge J. A., Stanford S. A., Richards G. T., 2011, ApJ, 736, 57
Zhang Y. et al., 2017, MNRAS, 468, 69

This paper has been typeset from a TEX/LATEX file prepared by the author.